13

Depth profiling of multilayer inhomogeneous ultra-thin films with a sub-nanometer resolution

© A.V. Lubenchenko,[1] O.I. Lubenchenko,[1] D.A. Ivanov,[1] D.S. Lukyantsev,[1] A.B. Pavolotsky,[2] O.N. Pavlov,[1] I.V. Ivanova[1]

[1] National Research University „MPEI"
111250 Moscow, Russia
[2] Chalmers University of Technology,
41296 Göteborg, Sweden
e-mail: LubenchenkoAV@mpei.ru

Received April 8, 2024
Revised April 8, 2024
Accepted April 8, 2024

A comprehensive in situ method of non-destructive quantitative chemical phase depth profiling of multilayer multicomponent ultra-thin films on various substrates is proposed, within sub-nanometer accuracy, for depth up to few tens nanometers, based on angle-resolved X-ray photoelectron spectroscopy and photoelectron energy losses spectroscopy. Chemical phase depth profiling of air-oxidized ultra-thin niobium and niobium nitride films has been performed.

Keywords: X-ray photoelectron spectroscopy, chemical and phase depth profiling, XPS background subtraction, XPS line decomposition.

DOI: 10.61011/TP.2024.08.59000.112-24

Introduction

Currently, layer-by-layer analysis of thin films is performed using both destructive and non-destructive methods. Standard methods for layer-by-layer analysis of thin films, such as secondary ion mass spectrometry(SIMS), transmission electron microscopy (TEM), scanning Auger microscopy(SAM), glow-discharge optical emission spectroscopy (GD-OES), X-ray photoelectron spectroscopy (XPS), Rutherford backscattering spectroscopy (RBS) and inductively coupled plasma and laser ablation mass spectrometry (LA-ICP-MS) are well developed and widely used in industrial and research laboratories. An overview of various nanometer-resolution layer analysis methods (RBS, SIMS, GD-OES, EBS, ERD, NRA) can be found in Ref. [1]. However, these methods are poorly suited for non-destructive analysis of ultra-thin films, as they are either destructive (for example, TEM, SIMS, GD-OES), or the depth resolution is on the order of or greater than the thickness of the ultra-thin films themselves (for example, RBS, SIMS).

Obtaining information about the layer-by-layer chemical composition of ultra-thin films at the nanometer level requires methods with high (subnanometer) resolution. XPS is one of the non-destructive methods of surface analysis which is highly sensitive to the surface and provides information about the elemental composition, chemical phase states and their distributions over depth.

As a rule, the near-surface region is not only multilayered, but it is also layered-multicomponent and multiphase. The depth profiling based on the interpretation of photoelectron spectra from such targets is a complex inverse problem with many previously unknown parameters. The following is proposed in Ref. [2] to correctly solve this problem:

1) the method of background subtraction taking into account the difference in energy losses of photoelectrons on the surface and in the volume;

2) the method of decomposition of a photoelectron line into its component peaks, taking into account the physical nature of various decomposition parameters;

3) the analytical formula for determining the layer thicknesses of a multilayer target.

It is necessary to know the sequence of target layers and the parameters of electron scattering in these layers to build a layer-by-layer profile. The information about this is not known in advance as a rule. It is proposed to use angular resolution X-ray photoelectron spectroscopy (AR XPS) (variations in the emission angles of photoelectrons occur due to the rotation of the target relative to the direction of view of the energy analyzer) and the characteristic energy loss spectra of photoelectrons taken in a wide range of energy losses with high resolution near the main photoelectron lines of the X-ray photoelectron spectrum for a more unambiguous resolution of the problem of layer distribution. Since there are several main photoelectron lines and they are formed by photoelectrons with different energies (the depth of sensing depends almost linearly on the initial electron energy), and inelastic scattering of photoelectrons occurs in layers with different depths, the order of arrangement, element and phase compositions of the layers will form a different background for each photoelectron line. Interpretation of the characteristic

energy loss spectra of photoelectrons is based on the background subtraction method in the case of a multilayer inhomogeneous medium.

The simultaneous analysis of photoelectron lines formed by non-scattered and elastically scattered electrons and the background for this line formed by inelastically scattered electrons at various sighting angles will allow for a reliable determination of layer-by-layer chemical phase profiles with sub-nanometer resolution.

1. Method of a layer-by-layer chemical phase analysis of multilayer inhomogeneous ultra-thin films

The method for solving the problem of determining the layer composition of multilayer inhomogeneous ultra-thin films with subnanometer resolution is based on:

1) background subtraction method for multi-layered inhomogeneous media;

2) general profile model of the X-ray photoelectron spectral line;

3) method for decomposing the X-ray photoelectron spectral line into phase spectral profiles;

4) model of a layered inhomogeneous target (determination of the number of layers, their composition and relative position; calculation of layer thicknesses using a simple formula).

1.1. Method of background subtraction in the case of a multilayer inhomogeneous medium

The following formula will be used to find the background $B(E)$ in the energy range from $E_{\min}$ to $E_{\max}$ for a spectral line from a multilayer target, taking into account the inhomogeneity of the sample, the difference in inelastic energy losses in the volume and on the surface of each layer

$$B(E) = \int_{E}^{E_{\max}} \Phi(x_{s1}(E-E'), SEP_1; x_{b1}(E-E'), d_1; \ldots) \times J^*(E')dE'. \quad (1)$$

Here $J^*(E) = J(E) - B_p(E)$, where $J(E)$ is the electron flux density determined from the experimental spectrum, $B_p(E)$ is the primary background determined from the preceding spectral line (or multiple lines); function $\Phi(\ldots)$ is the generalized inelastic energy loss function; $x\Delta$ is the single inelastic energy loss function (orthonormalized inelastic scattering differential cross section or probability density of losing energy by single inelastic scattering); Δ is the energy loss; the numbers in the lower index indicate in which layer the energy loss occurs; the index „s“ corresponds to the energy loss on the surface of the i-th layer; the index „b“ corresponds to energy loss in the volume of the i-th layer; SEP_i is the surface excitation parameter of the i-th layer (the parameter SEP depends on the photoelectron energy, composition and state of the surface); d_i is the thickness of the i-th layer.

Such a background subtraction structure (1) was first applied by Tougaard [3], but his approach took into account only multiple inelastic scattering of electrons in the volume of a semi-infinite medium. Tougaard used the three-parameter formula as a generalized inelastic loss function

$$\Phi(\Delta) = x_b(\Delta) = A\frac{\Delta}{(C-\Delta^2)^2 + D\Delta^2}, \quad (2)$$

where A, C and D are the fitting parameters.

The paper [2] presents a background subtraction method that takes into account multiple inelastic scattering on the surface and in the volume of a semi-infinite medium. A term describing inelastic scattering in near-surface layers and correlation of inelastic scattering in the volume and on the surface is added to the Tougaard background:

$$\Phi(\Delta) = x_b(\Delta) + L_{sb}(\Delta), \quad (3)$$

where $x_b(\Delta)$ is a function of single inelastic losses in the volume, $L_{sb}(\Delta)$ is a function describing inelastic scattering in near-surface layers and the correlation of inelastic scattering in the volume and on the surface.

The generalized inelastic loss functions listed above were obtained for a semi-infinite medium without taking into account differences in the laws of energy loss on the surface and in volume ($SEP = 0$, formula (2)) and for a semi-infinite medium with taking into account differences in energy losses on the surface and in volume ($SEP \neq 0$, formula (3)). However, real surfaces are multi-layered and inhomogeneous. A method of background subtraction in the case of a multi-layered inhomogeneous medium is required to accurately interpret X-ray photoelectron spectra from real targets.

Let us introduce a target model consisting of flat homogeneous layers with thicknesses of $d_1, \ldots d_N$deposited on a semi-infinite substrate for constructing a background subtraction method in the case of a multilayer inhomogeneous medium. A bottom-up approach will be used for numbering. The digit 0 corresponds to the substrate. The laws of inelastic single energy losses of photoelectrons in the volume $x_b(\Delta)$ and in the near-surface layer $x_s(\Delta)$ should be determined in each layer. Let us consider the photoelectron emission from the i-th layer. When the target is illuminated by a flux of X-ray photons with an energy of $h\nu$ at an angle of α to the surface normal, electrons are produced inside the i-th layer with an energy of E_0 evenly over the entire layer. The photoelectron moves in a straight line from the point of origin to the exit from the target surface and does not experience elastic scattering leading to a change of direction („straight−forward“ or straight line approximation (SLA) [4]). The flux density of such photoelectrons will be determined by the formula (Fig. 1):

$$q_{i\ldots N}(z, \Delta) = n_i \omega_{h\nu \to ei}(\psi) T_{i\ldots N}(z, \Delta), \quad (4)$$

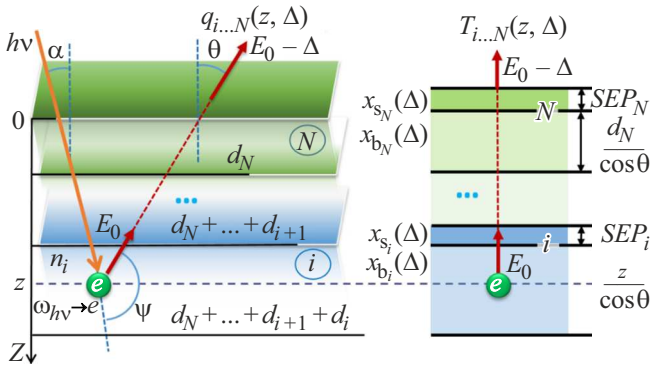

Figure 1. Photoelectron emission from the i-th layer of a multilayer target.

where n_i is the concentration of atoms in the i-th layer; $\omega_{h\nu \to ei}(\psi)$ is the differential cross-section of photoelectron generation in the i-th layer; ψ is the angle between the directions of the photon incident on the atom and the photoelectron flying out of the atom; $T_{i...N}(z, \Delta)$ is the function of multiple inelastic energy losses when a photoelectron passes through an inhomogeneous medium from the point of origin to the point of departure (inelastic transmission function).

The flux density of all photoelectrons produced in the i-th layer and released from the target, $Q_{i...N}(\Delta)$ (photoelectron emission function), will be determined by the integral over all depths up to the lower boundary of the i-th layer:

$$Q_{i...N}(\Delta) = \int_0^{d_i + ... + d_N} q_{i...N}(z, \Delta) dz. \tag{5}$$

Since photoelectrons are generated in the i-th layer, integration should only be performed over the thickness of the i-th layer. Let us integrate the formula (5) and transform it to the form in which a part of the function $P(\Delta)$ describing the flux of photoelectrons that have not lost the energy is explicitly distinguished, and the other part is the background $B(\Delta)$ formed by repeatedly inelastically scattered photoelectrons:

$$Q_{i...N}(\Delta) = P(\Delta) + B(\Delta) = Q_{\text{eli}} e^{-\tau_{\text{tot}}} \delta(\Delta)$$
$$+ Q_{\text{eli}} e^{-\tau_{\text{tot}}} \left(e^{\tau_{\text{tot}}} \int_0^{d_i/\lambda_i \cos\theta} T_{\text{bi}}(\tau, \Delta) d\tau \right.$$
$$\left. \otimes T_{i+1,...,N}(SEP_i, d_{i+1}, SEP_{i+1}, \ldots, d_N, SEP_N, \Delta) - \delta(\Delta) \right). \tag{6}$$

Here $T_{i+1,...,N}(SEP_i, d_{i+1}, SEP_{i+1}, \ldots, d_N, SEP_N, \Delta)$ — inelastic function of transmission by layers located above the i-th layer (Fig. 1); $Q_{\text{eli}} = n_i \omega_{h\nu \to ei}(\psi) \lambda_i \cos\theta$ is function of photoelectron emission from a semi-infinite medium consisting of the material of the i-th layer, electrons that have not lost energy; $\tau_{\text{tot}} = SEP_i + \sum_{j=i+1}^{N} (SEP_j + \tau_j)$ — dimensionless total thickness of layers above the i-th layer; $\tau_j = d_j/(\lambda_j \cos\theta)$ is a dimensionless thickness of the j-th layer; λ is the inelastic mean free path (IMFP); $\delta(\Delta)$ is the Dirac delta function.

The photoelectron emission function $Q_{i...N}(\Delta)$ is proportional to the photoelectron flux density $J(E)$ determined from the experimental spectrum. Let us find a generalized inelastic loss function for a multilayer target from expressions (6) and (1) on condition that $d_i > \lambda_i \cos\theta$:

$$\Phi(\Delta) = x_{b_i}(\Delta) - L(\Delta) \otimes x_{b_i}(\Delta) + L(\Delta), \tag{7}$$

where the function $L(\Delta)$ is calculated by formula

$$L(\Delta) = T_{i+1,...,N}(SEP_i, d_{i+1}, SEP_{i+1}, \ldots, d_N, SEP_N, \Delta) e^{\tau_{\text{tot}}}$$
$$- \delta(\Delta) = \sum_{n=1}^{K} (-1)^{n+1} \frac{\tau_{\text{tot}}^n}{n!} y_n(\Delta), \tag{8}$$

where K is the maximum multiplicity of inelastic scattering taken into account; $y_n(\Delta)$ — function of n-fold inelastic scatterings, $y_n(\Delta) = y_{n-1}(\Delta) \otimes y_1(\Delta)$,

$$y_1(\Delta) = \frac{SEP_i}{\tau_{\text{tot}}} x_{si}(\Delta) + \sum_{j=i+1}^{N} \left(\frac{SEP_j}{\tau_{\text{tot}}} x_{sj}(\Delta) + \frac{\tau_j}{\tau_{\text{tot}}} x_{bj}(\Delta) \right). \tag{9}$$

The function $y_1(\Delta)$ can be interpreted as the average function of single inelastic energy losses.

Tougaard formula (2) will be obtained provided that the target consists of a semi-infinite medium in formula (7) and the surface energy losses ($SEP = 0$) are ignored. We get the formula (3) if we also add the calculation of surface energy losses ($SEP \neq 0$).

The inelastic scattering involves the interaction of an electron with electrons of a solid body, accompanied by a small momentum transfer and large energy losses compared to the recoil energy losses in elastic collisions. The reaction of the electronic subsystem of a solid body to an energy impact, depending on the energy of incident electrons, proceeds through various excitation channels, including collective plasma vibrations, ionization of the inner shell, proper and inter - or intra-band transitions.

The single inelastic energy loss function $x(\Delta)$ can be calculated within the framework of the complex permittivity formalism $\varepsilon(\Delta, q)$ and (q and Δ are the momentum and energy transferred to the system):

$$x(\Delta) = \frac{1}{\lambda} \frac{1}{\pi E_0} \int_{q_-}^{q_+} \text{Im}\left(-\frac{1}{\varepsilon(\Delta, q)} \right) \frac{dq}{q}. \tag{10}$$

Atomic units ($\hbar = e = m_e = 1$) are used in the expression (10). The dimensionless value $\text{Im}(-1/\varepsilon(\Delta, q))$ in the formula (10) is the so-called energy loss function (ELF). The integration limits, which depend on both the initial energy E_0 and the energy loss Δ, are a consequence of conservation of energy and momentum:

$$q_{\pm} = \sqrt{2E_0} \pm \sqrt{2(E_0 - \Delta)}. \tag{11}$$

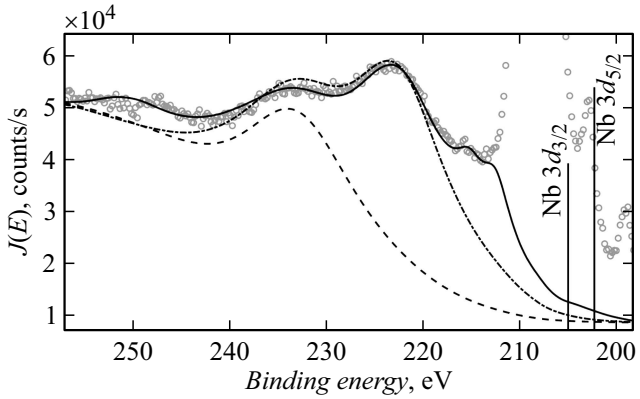

Figure 2. Spectrum of characteristic energy losses of photoelectrons of the Nb 3*d* line from an oxidized niobium film.

The statistical electron gas model, which is usually called the Drude–Lindhard model is one of the widely used approaches to description. The imaginary part of the inverse dielectric function $\mathrm{Im}(-1/\varepsilon(\Delta, q))$ is given in this approach as [5]:

$$\mathrm{Im}\left(-\frac{1}{\varepsilon(\Delta, q)}\right) = \sum_i C_i \frac{\Delta\gamma_i E_{pi}^2}{\left(\Delta^2 - (E_{pi} + \alpha q^2/2m_e)^2\right)^2 + \Delta^2\gamma_i^2}, \quad (12)$$

where E_p is the energy of plasma oscillations; γ is the excitation attenuation energy width (γ is inversely proportional to the excitation lifetime); α — constant in the range from 0 to 1 (for metals $\alpha = 1$, for dielectrics $\alpha = 0$); C are the weighting factors; index i corresponds to certain regions of matter having different electron gas densities. It should be noted comparing formulas (12) and (9) that the weighting factors C_i are proportional to the dimensionless layer thicknesses in the multilayer target model, and the presence of several plasma oscillation energies can be explained by the excitation of plasma oscillations in different layers during photoelectron scattering in inhomogeneous multilayer media.

Figure 2 shows the spectrum of characteristic energy losses of photoelectrons of the Nb 3*d* line from an oxidized niobium film with a thickness of 10 nm. Circles show experimental data, dashed line shows the background calculation using the model of homogeneous semi-infinite medium without considering surface energy losses ($SEP = 0$), dashed line shows the background calculation using the model of homogeneous semi-infinite medium with consideration of surface energy losses ($SEP \neq 0$), solid line shows the background calculation using the two-layer multicomponent target model.

1.2. General profile model of the X-ray photoelectron spectral line

The measured signal is formed in XPS by electron fluxes emitted by the target and passing through the energy analyzer and detector system. This system distorts the original signal. For taking them into account it is necessary to know the apparatus function of the measuring system $f_\mathrm{ms}(E, w_\mathrm{ms})$ (E is the kinetic energy of the photoelectron, w_ms is the apparatus broadening associated with the measuring system), the primary photoelectron emission function $f_\mathrm{e}(E, w_\mathrm{n}, E_\mathrm{so}, \alpha, E_\mathrm{cs})$, which takes into account the photoelectron energy distribution attributable to the intrinsic electron level width, spin-orbit interaction, and chemical shift (w_n is the intrinsic electron level width, E_so is the spin-orbit interaction energy, α is the ratio of intensities of spin-orbit splitting lines of photoelectron level, ΔE_cs is the chemical shift energy), and the X-ray gun instrument function $f_g(E, w_\mathrm{g}, \Delta E_\mathrm{sat}, \alpha_\mathrm{sat})$ (w_g — apparatus broadening associated with the X-ray gun, ΔE_sat is the satellite peak shift energy, α_sat are the relative intensities of satellite peaks).

The flux density of elastically scattered and non-scattered photoelectrons (the general profile of the photoelectron spectral line) will be determined by the convolution of the instrument function of the X-ray gun, the primary photoelectron emission function, and the instrument function of the measuring system:

$$P(E) = \int_E^{E_\mathrm{max}} \int_E^{\prime E} f_\mathrm{g}(E - E', w_\mathrm{g}, \Delta E_\mathrm{sat}, \alpha_\mathrm{sat}) f_e(E' - E'', w_\mathrm{n}, E_\mathrm{so}, \alpha, \Delta E_\mathrm{cs}) f_\mathrm{ms}(E'', w_\mathrm{ms}) dE' dE''. \quad (13)$$

Here the energy changes in the given energy range (region) — from E_min to E_max.

The instrument function of the measurement system and the apparatus function of the X-ray gun are well described by the Gaussian function.

The spectral line profile of photoelectrons emitted by atoms in the same chemical state is approximated by the Lorentz function. The profile of the spectral line of photoelectrons can have an asymmetric (beveled) shape. This is attributable to the fact that photoionization in some materials (for example, simple and noble metals) can be accompanied by a number of multi-electron effects, in which photoelectrons lose energy, which ultimately results in an asymmetry. The shape of a core-level photoelectron line with a natural width of w_n in this case is described by convolution of the Lorentz function (5) and the singular function. Doniach and Sunjic in [6] obtained an approximate formula for such a convolution. The photoelectron peaks formed by electrons with p-, d-, f-, ... shells due to the spin-orbit interaction form a doublet structure. The spectral photoelectron line formed by photoelectrons emitted by a chemically bound atom will be shifted by the chemical shift energy E_cs. The chemical shift energy depends on the oxidation level z of the element in the compound. If the sample contains atoms of the same chemical element with different oxidation levels, the spectral photoelectron line will be formed by peaks (taking into account spin-orbit and/or multiplet splitting) attributable to each of these bound states.

The expression for the general profile of the X-ray photoelectron spectral line is obtained by substituting all the previously considered functions into the formula (13):

$$P(E) = \sum_k \sum_i \sum_j I_k \beta_i A_{\text{sat}\,j} f_{\text{VoigtDS}}(E - (E_{\text{k}i} - E_{\text{so}i} - E_{\text{cs}k} + \Delta E_{\text{sat}\,j}), w_{\text{gms}}, w_{\text{n}i,k}, \alpha_{\text{A}k}). \quad (14)$$

Here $f_{\text{VoigtDS}}(\ldots)$ is the convolution of the Gaussian function with the Doniach–Sunjic function (when $\alpha_{\text{A}} = 0$ convolution passes into the Voigt function); E_{k} is the photoelectron initial kinetic energy; $w_{\text{gms}} = \sqrt{w_{\text{g}}^2 + w_{\text{ms}}^2}$ — total apparatus broadening equal to the root-mean-square apparatus broadening of the X-ray gun and measuring system; $A_{\text{sat}\,j}$, $\Delta E_{\text{sat}\,j}$ — relative intensity and shift of the j-th satellite peak; β_i, $E_{\text{so}i}$ — relative contribution and energy of the i-th peak due to spin-orbit or multiplet splitting; I_k, $\Delta E_{\text{sc}k}$, $w_{\text{n}}i, k$, $\alpha_{\text{A}}k$ — relative intensity, chemical shift energy, natural level width, the Anderson coefficient of the k-th peak due to the bound state of the element with an oxidation state of z (for a chemically pure element $z = 0$).

The number of satellite peaks and their parameters (relative intensity A_{sat} and displacement ΔE_{sat}) depend on the X-ray gun and are determined using the experimentally measured X-ray photoelectron spectra from chemically pure targets (usually silver or gold samples are used). We propose to find the relative contribution β and the energy of the peak E_{so} attributable to spin-orbit or multiplet splitting, as well as the natural broadening of the energy level line of a chemically pure element $w_{\text{n}}0$ and the Anderson coefficient $\alpha_{\text{A}}0$ from the results of interpretation of X-ray photoelectron spectra from pure homogeneous targets from Handbook of X-Ray Photoelectron Spectroscopy [7] using the formula of the general profile of the spectral line (14) after subtracting the background using the method (1), using (7).

The values of chemical shift energies for various compounds can be found in the NIST database [8]. A solid line in Figure 3 shows a linear approximation of the dependence of the chemical shift of the Nb 3d line on the oxidation level z of niobium, circles show the data from NIST [8]. This approximation is expressed by the formula

$$\Delta E_{\text{sc}} + E_{\text{sc}1} z, \quad (15)$$

where $E_{\text{sc}1}$ is the chemical shift energy per oxidation level, $E_{\text{sc}1} = 1.06$ eV for Nb 3d line. There are several theoretical approaches for calculating the chemical shift energy. One approach relies on the binary Miedema alloy model [9] and the Born–Haber cycle [10]. The density functional method is used in the other approach. An example of calculation of the chemical shift energy using the density functional method for Me–N_x is given in the article in Ref. [11].

The approximate formula can be used to determine the dependence of the natural width of the energy level

$$w_{\text{n}} = w_{\text{n}0}\rho^z, \quad (16)$$

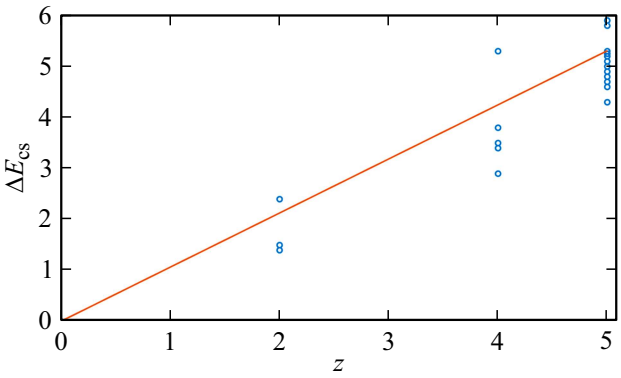

Figure 3. Dependence of the chemical shift of the Nb 3d line depends on the oxidation level of niobium.

where $w_{\text{n}0}$ is the natural width of the energy level of a chemically pure element, ρ is parameter ($\rho \geq 1$), $\rho = 1.07$ for the line Nb 3d.

Let us call as phase functions the parameters (I_k, $E_{\text{sc}k}$, $w_{\text{n}i,k}$, $\alpha_{\text{A}k}$) attributable to the bound or chemically pure state of the element. The phase means the region of a substance that has the same chemical, physical, and crystallographic properties.

Let us call the sum of peaks describing the spectral profile for one phase state the phase spectral profile

$$P_k(E) = I_k \sum_i \sum_j \beta_i A_{\text{sat}\,j} f_{\text{VoigtDS}}(E - (E_{\text{k}i} - E_{\text{so}i} - E_{\text{cs}1} z_k + \Delta E_{\text{sat}\,j}), w_{\text{gms}}, w_{\text{n}0}\rho^{z_k}, \alpha_{\text{A}k}). \quad (17)$$

Then the total profile of the spectral line from (13) and (17), taking into account (15) and (16), will consist of the sum of the phase spectral profiles (K is the number of phases):

$$P(E) = \sum_{k=1}^{K} P_k(E, I_k, z_k). \quad (18)$$

Fig. 4 shows the profile of the spectral line Nb 3d: a solid line in Fig. 4, a shows the primary emission function; a solid line in fig. 4, b shows the total profile. The color fill shows partial peaks corresponding to different niobium oxidation levels. The calculation was performed for a non-monochromatic X-ray gun using Mg anode. Decomposition parameters: bond energy of Nb 3d $E_{\text{b}} = 202.3$ eV; spin-orbit interaction energy $E_{\text{so}} = 2.75$ eV; natural linewidth $w_{\text{n}0} = 0.32$ eV; apparatus broadening associated with the X-ray gun, $w_{\text{g}} = 0.29$ eV; instrumental broadening associated with the measurement system, $w_{\text{ms}} = 0.38$ eV; $E_{\text{cs}1} = 1.06$ eV; $\rho = 1.07$. The phases were set in the calculation: metal Nb, NbO_2, Nb_2O_5. Ratio of peak phase intensities: $I_{\text{Nb}} : I_{\text{Nb O}_2} : I_{\text{Nb}_2}\text{O}_5 = 1 : 2 : 4$.

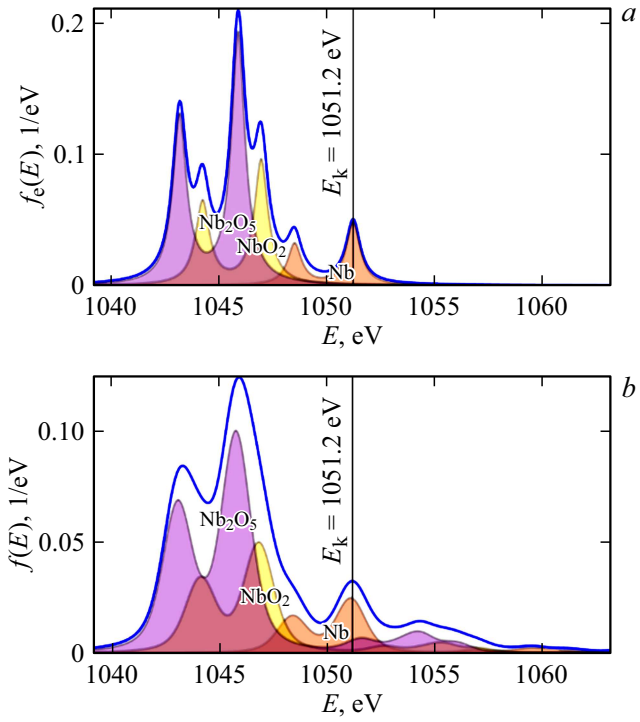

Figure 4. Profile of photoelectron spectral line Nb 3*d*.

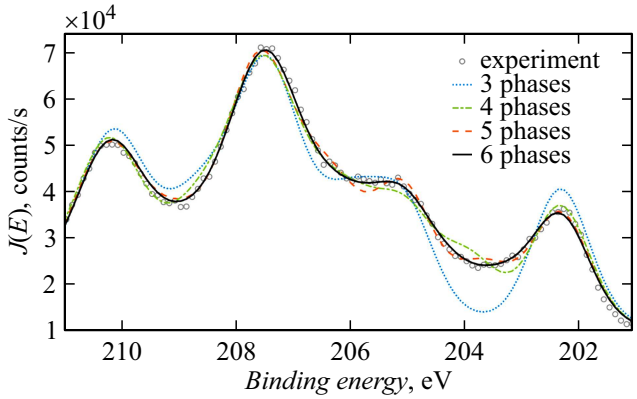

Figure 5. Calculated X-ray photoelectron spectrum as a function of the number of phases K in case of decomposition of the spectral X-ray photoelectron line Nb 3*d*.

1.3. Method of decomposition of the X-ray photoelectron spectral line into phase spectral profiles

The theoretical X-ray photoelectron spectrum consists of the general profile of the spectral line and the background:

$$S_{\text{theor}}(K, E) = \sum_{k=1}^{K} P_k(E, I_k, z_k)$$

$$+ \int_{E}^{E_{\max}}]\Phi(x_{s1}(E-E'), SEP_1; x_{b\,1}(E-E'),\ d_1; \ldots) J^*(E')dE'. \tag{19}$$

Here $J^*(E)$ is the electron flux density determined from the experimental spectrum in the energy range from $E_{\min}$ to $E_{\max}$.

The conformance of the experimental spectrum and the theoretical spectrum will be evaluated by chi-square over the entire measured spectrum:

$$\chi^2(K) = \sum_i \frac{(S_{\text{theor}}(K, E_i) - J^*(E_i))^2}{J^*(E_i)}. \tag{20}$$

The phase parameters for a given number of phases K and the background parameters can be found by the least squares method with chi-square minimization.

The minimum chi-square value depends on the number of phases K. If the addition of a phase does not significantly reduce the minimum chi-square value, then the number of phases will be sufficient.

Figure 5 shows the dependences of theoretical X-ray photoelectron spectra on the number of phases K in case of decomposition of the spectral X-ray photoelectron line Nb 3*d*. Circles represent the experiment, dots show the theoretical spectrum for 3 phases, dashpoint show the theoretical spectrum for 4 phases, dotted line shows the theoretical spectrum for 5 phases, solid line shows the theoretical spectrum for 6 phases. Table 1 shows the bond energies of E_b and the oxidation degrees of z k-phases as a function of the number of phases K. Values of the bond energy E_b and oxidation levels z were obtained by minimizing the chi-square with a given K. The table shows the minimum chi-square values with a given K. The best decomposition is achieved with $K = 6$. Knowing the oxidation level it is possible to determine the chemical formula of the oxide for the k-th phase. These formulas are given in Table 1.

1.4. Layered inhomogeneous target model

It is necessary to create a target model describing this surface for layer-by-layer analysis of a solid body surface. The measured XPS spectrum is formed by a target region with an area of 1 mm^2, whose characteristic dimensions are orders of magnitude larger than the probing depth (about 10 nm). The XPS signal is averaged horizontally in this case, but not vertically. Then it is possible to use a target model consisting of several plane-parallel homogeneous layers with a thickness of the order of nanometers deposited on a semi-infinite substrate. In this model, horizontal inhomogeneities (islands, interlayer roughnesses, inclusions, etc.) are averaged over a layer whose effective thickness may be less than the monolayer thickness (about 0.5 nm).

Each layer in a multi-layer target can be multicomponent. The relative concentration of a component (bound element) in a layer can be calculated from the phase relative intensities of the spectral lines of the components determined after the procedure for decomposing the X-ray photoelectron spectral line into phase spectral profiles.

Table 1. Binding energy BE and oxidation level z k-th phase depending on the number of phases K in case of decomposition of the spectral X-ray photoelectron line Nb 3d

k	$K=3$		$K=4$		$K=5$		$K=6$		
	z	BE, eV	z	BE, eV	z	BE, eV	z	BE, eV	Formula
1	0	202.3	0	202.3	0	202.3	0	202.3	Nb
2	3.5	205.9	1.6	203.9	1.3	203.6	1.0	203.3	Nb_2O
3	4.9	207.3	3.5	205.9	2.8	205.1	1.9	204.2	NbO
4			4.9	207.4	3.9	206.3	3.1	205.5	Nb_2O_3
5					5.0	207.4	3.9	206.3	NbO_2
6							5.0	207.4	Nb_2O_5
χ^2	12.8167		2.4765		1.6769		1.0877		

The order of layers (target structure) becomes particularly important in this target model. This order is either determined in advance (from knowledge of the creation history and subsequent „life“ of the target), or follows from the processing of the results of several XPS experiments with this target (for example, XPS with angular resolution, [12]). The probing depth (information depth) will decrease proportionally to $\cos\theta$ with an increased sighting angle θ. In this case, the contribution of phases located near the surface boundary to the overall profile of the X-ray photoelectron spectral line will be more significant than the contribution of phases located in the sample depth. It is possible to make an assumption about the order of arrangement of layers with a particular phase by performing measurements at different sighting angles and decomposing X-ray photoelectron spectral lines at different angles into phase spectral profiles.

The accuracy of calculating the layer composition of the studied film depends on the choice of the background subtraction method. In turn, it is necessary to know the layer composition of the sample to accurately describe the background formed by inelastically scattered photoelectrons. We will use an iterative approach to solve this problem. First, we use the method of subtracting the background from a semi-infinite homogeneous medium with energy losses in the volume and on the surface; after determining the layer composition, we obtain a layer-by-layer profile in the first approximation. Next, let us select the main layer and use the background subtraction method for the „substrate–layer“ system and obtain the profile in second approximation. Let us use the background subtraction method for a multi-layered inhomogeneous medium at the third stage.

Let us introduce the minimum thickness of a homogeneous layer equal to the average distance between monolayers in a solid (about 0.5 nm) to reduce the uncertainty of the number of layers. The calculation starts with the maximum possible number of layers, assuming that the oxidation level of the main element(-s) is the same in each layer. If the calculation shows that a certain layer has a thickness less than the minimum, then this layer is joined to the nearest layer in which the oxidation level of the main element is greater. The newly formed layer will be multicomponent with some effective thickness. The layer thicknesses are recalculated after that. This approach allows for a significant reduction of the number of calculation options treating the options themselves as profiles calculated with different depth accuracy.

The thickness of a multilayer model will be determined based on the approach described in Ref. [2]. The thickness of the i-th layer is calculated using a simple formula

$$d_i = \lambda_i \cos\theta \ln\left[\frac{I_i/(n_i\omega_{h\nu\to ei}(\psi)\lambda_i)}{\sum_{j=0}^{i-1} I_j/(n_j\omega_{h\nu\to ej}(\psi)\lambda_j)} + 1\right], \qquad (21)$$

where I_i is phase relative intensity in the i-th layer; n_i is the atomic concentration in the i-th layer; λ is inelastic mean free path (IMFP); $\omega_{h\nu\to ei}(\psi)$ is the differential cross-section of photoelectron generation in the i-th layer; ψ is the angle between the directions of the photon incident on the atom and the photoelectron escaping the atom.

The formula (21) for calculating layer thicknesses was derived for photoelectrons that, after birth, do not experience elastic scattering resulting in a change of the motion direction (SLA). However, multiple elastic scattering can weaken the flow of electrons moving in a straight line. The Effective Attenuation Length (EAL) approximation is used to take into account this impact. In this approximation, the parameter L_{eff} being the effective attenuation length is substituted for the average length of the free inelastic path in the formula for the layer thicknesses calculation. The values L_{eff} may be different when used in different analytical procedures.

It is shown in the paper of A. Yablonsky [13] that it is necessary to introduce different effective attenuation lengths

for a photoelectron moving in a thin layer L_{th} and in a semi-infinite medium L_{qa}:

$$L_{\text{th}} = (1 - 0,738\Lambda)\lambda, \quad L_{\text{qa}} = (1 - 0,147\Lambda - 0,164\Lambda^2)\lambda, \tag{22}$$

where $\Lambda = \lambda/(\lambda + \lambda_{\text{tr}})$, λ_{tr} — transport mean free path (TRMFP) of a photoelectron in substance.

Let us modify the formula for calculating the thickness of the i-th layer taking into account multiple elastic scattering using (22):

$$d_i = L_{\text{th}i} \cos\theta \ln\left[\frac{I_i/(n_i\omega_{\gamma\to ei}L_{\text{qa}i})}{\sum\limits_{j=0}^{i-1} I_j/(n_j\omega_{\gamma\to ej}L_{\text{qa}j})} + 1\right]. \tag{23}$$

Let us determine the probing depth (information depth) d_{inf} — the maximum layer thickness in the target „layer–substrate“, which can be found using the formula (23) in case of the ratio $I_1/I_0 = 100$. This ratio is taken from considerations that we determine the phase intensities with an accuracy of 1%. Let us assume that the products $n_1\omega_{\gamma\to e1}\lambda_1 \approx n_0\omega_{\gamma\to e0}\lambda_0$. Then the following is obtained from the formula (23)

$$d_{\text{inf}} = 4.62\lambda_1 \cos\theta. \tag{24}$$

Let us assume the ratio $I_1/I_0 = 0.01$ for determination of the minimum possible thickness. Then the following is obtained from the formula (23)

$$d_{\text{min}} = 0.01\lambda_1 \cos\theta. \tag{25}$$

The mean free path of a photoelectron is about 2 nm. In this case, the minimum thickness of the averaged layer that can be determined using this method, it has a value of about 0.02 nm, or 0.04 monolayer. If the layer thickness is less than 1 monolayer, then this indicates the island structure of the layer itself. Therefore, the method presented in this paper for determining the layer composition has a subnanometer resolution.

2. Layer-by-layer chemical phase analysis of an oxidized ultra-thin niobium film

X-ray photoelectron spectra were obtained using the electron-ion spectroscopy module based on the Nanofab 25 (NT-MDT) platform. An ultra-high oil-free vacuum of the order of 10^{-6} Pa was achieved in the analytical chamber. The spectra were taken with an electrostatic hemispherical energy analyzer SPECS Phoibos 225 using an X-ray gun with Mg anode. Calibration of the energy analyzer was performed using samples from Cu, Ag and Au. The energy resolution of the spectrometer along the line Ag $3d_{5/2}$ was 0.78 eV (width at half maximum) for non-monochromatic X-ray radiation of Mg Kα. The energy analyzer operated in the FAT mode (Fixed Analyzer Transmission). The deceleration energy in the energy analyzer lens of $E_{\text{pass}} = 80$ eV was determined for survey spectra, for detailed spectra it was equal to $E_{\text{pass}} = 20$ eV.

2.1. An air-oxidized ultra-thin niobium film on a silicon substrate

The niobium film was deposited on a silicon substrate by magnetron sputtering in a Pfeiffer Vacuum SLS630G. The film thickness during sputtering was controlled by the known sputtering rate (the sputtering rate was confirmed by the TEM method). The film was air-oxidized after unloading from the chamber.

The elements Nb (31.4%), O (58.4%), and C (10.2%) were detected on a silicon substrate during the XPS elemental analysis of an ultra-thin niobium film oxidized in air. No silicon was detected. This indicates that the depth of silicon occurrence in the target is greater than the probing depth (information depth). The phase analysis will be performed using the method of decomposition of the X-ray photoelectron spectral line into the phase spectral profiles. Since the elements niobium and oxygen are found in the film, it should contain various niobium phases: metallic niobium, niobium suboxides, and higher niobium oxide. Carbon is found in near-surface layers deposited from air. No chemical bonds of niobium with carbon were detected. The phases Nb, Nb_2O, NbO, Nb_2O_3, NbO_2, Nb_2O_5 were found by the decomposition of the X-ray photoelectron spectral line (Fig. 5). The X-ray photoelectron spectrum of the Nb $3d$ line of an oxidized ultra-thin niobium film is shown on Fig. 6. Circles indicate experimental data, solid line indicates the theoretical interpretation of the spectrum, shaded areas show the phase spectral profiles, dashed line shows the background. The background was calculated using a two-layer multicomponent target model (Fig. 2).

The information depth of the analysis depends on the substance and the sighting angle. It is equal to 9.6 nm for a niobium oxide target at a sighting angle of 0°, it is equal to

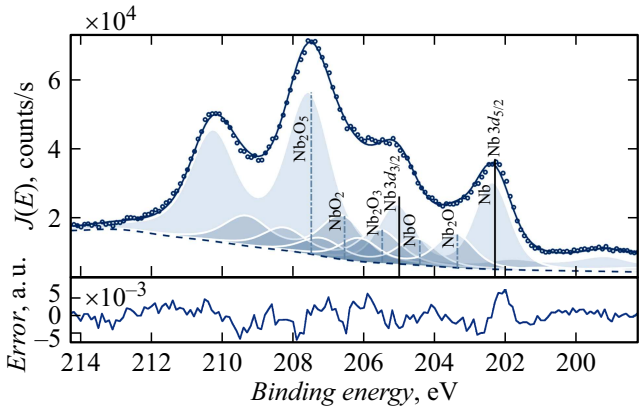

Figure 6. X-ray photoelectron spectrum of the Nb $3d$ line from an oxidized niobium film.

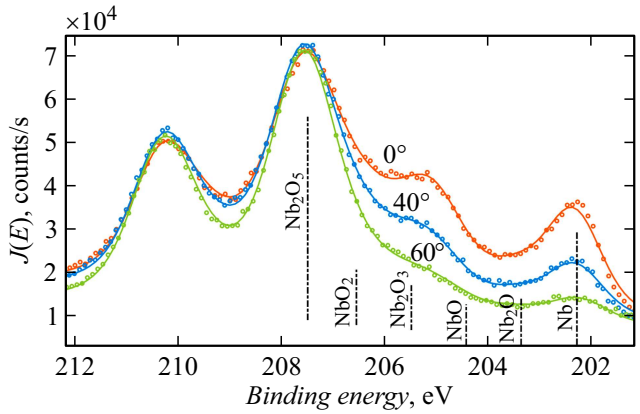

Figure 7. X-ray photoelectron spectrum of the Nb 3*d* line from an oxidized niobium film at various sighting angles.

7.4 nm at a sighting angle of 40° and to 4.8 nm at a sighting angle of 60°.

The phase analysis shows that the relative intensity of the peaks corresponding to the phase N_2O_5 significantly increases with the increase of the sighting angle, the relative intensities of the peaks of phases NbO_2 and Nb_2O_3 slightly increase, the relative intensities of the peaks of phases Nb_2O and NbO decrease, the relative intensity of the peaks of phase Nb strongly decreases. This allows proposing a target model consisting of 4 layers on a silicon substrate: the lower layer 1 consists of Nb, layer 2 consists of Nb_2O and NbO, layer 3 consists of NbO_2 and Nb_2O_3, top layer 4 consists of Nb_2O_5.

Fig. 7 shows the X-ray photoelectron spectra of the Nb 3*d* line of the oxidized ultra-thin niobium film at different sighting angles of 0°, 40° and 60°. Experimental data are shown by circles, calculated data are shown by the solid line.

Layer thicknesses are calculated using the formula (23). The calculation results are given in Table 2. Layer thicknesses calculated for different sighting angles are the same. This indicates the adequacy of the selected target model.

2.2. An air-oxidized ultra-thin niobium nitride film with a gallium nitride buffer layer on a sapphire substrate

The process of creating niobium nitride films on gallium nitride is described in [14]. A gallium nitride buffer layer was grown on a sapphire base by chemical vapour deposition. Niobium nitride films were created using an Orion magnetron sputtering system manufactured by AJA International Inc. A metallic niobium target (purity 99.9%) was sputtered in the argon and nitrogen atmosphere (N_2). The relative nitrogen concentration in the mixture was 89.1%. The sputtering was carried out at room temperature at a rate of 1.2 Å/s.

The obtained films were controlled by high-resolution transmission electron microscopy (HRTEM). The image (Fig. 8) taken from Ref. [14] shows that niobium nitride and gallium nitride have a single-crystal structure and their crystal lattices almost exactly match. The thickness of niobium nitride layer is approximately 5 nm.

The same ultra-thin niobium nitride film with a gallium nitride buffer layer on a sapphire substrate as in Ref. [14] was studied by the XPS method.

The following elements were detected during the element analysis of NbN/GaN/Sp films: Nb (40.5%), O (38.7%), N (16.2%), Ga (1.4%), residual traces of C (2.4%) and Na (0.8%). Aluminum was not detected. Thus, the thickness of the layers above the sapphire substrate is greater than the probing depth.

The phase analysis of ultra-thin NbN/GaN films on a Sp substrate is performed simultaneously on spectral photoelectron lines of N 1*s*, O 1*s*, Nb 3*d*, Ga 3*d*. Various phases of niobium nitride NbN and NbN_x were determined by the analysis of photoelectron lines of N 1*s* and Nb 3*d*; niobium oxides and suboxides NbO_2, Nb_2O_5 were determined by the analysis of photoelectron lines of lines O 1*s* and Nb 3*d*; different phases of gallium nitride GaN and GaN_x were determined by the analysis of photoelectron lines of N 1*s*, Ga 3*d*.

X-ray photoelectron spectra of Nb 3*d* lines of the NBN/GaN/Sp ultra-thin film are shown on Fig. 9. Solid line shows the calculated spectra, circles show the experiment data, dashed line shows the background calculated using the method considered in this paper, phase spectral lines are shown by the fill: NbN, NbN_x, NbO_2, Nb_2O_5.

Let us introduce a target model for layer-by-layer analysis. It known from the history of its creation that niobium was sputtered in the nitrogen and argon atmosphere over a gallium nitride film on a sapphire substrate. Then the atmospheric oxidation occurred, and a niobium oxide film was formed on top. So the target model will consist of three layers. The base is formed by a layer of gallium nitride on a sapphire substrate, then there is a niobium nitride film and an oxide layer on top. Table 3 shows the layer-by-layer chemical phase profile of the oxidized NbN/GaN/Sp film. The thickness of the niobium nitride layer is 5.3 ± 0.4 nm.

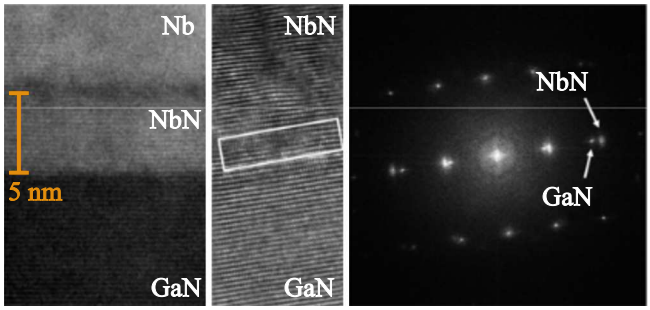

Figure 8. The cross-sectional image of the NbN/GaN film obtained by the HRTEM method HRTEM [14].

Table 2. Layer-by-layer chemical phase profile of the oxidized film for different sighting angles of 0°, 40° and 60°

№	d, nm			Chemical formula
	0°	40°	60°	
4	2.4 ± 0.3	2.4 ± 0.3	2.33 ± 0.21	Nb_2O_5
3	1.25 ± 0.19	1.27 ± 0.18	0.94 ± 0.13	$0.56Nb_2O_3 + 0.44NbO_2$
2	1.50 ± 0.22	1.30 ± 0.18	1.26 ± 0.16	$0.55Nb_2O + 0.45NbO$
1	Thickness not determined			Nb

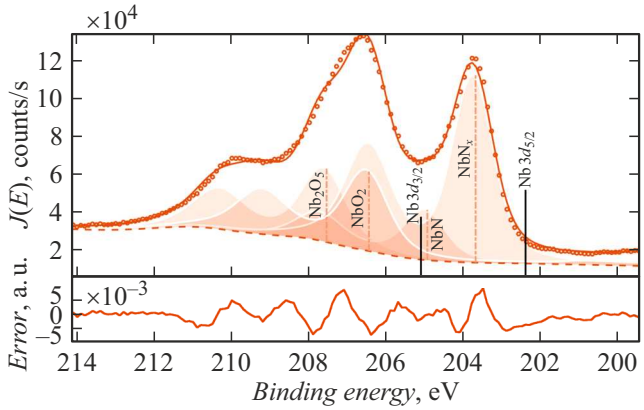

Figure 9. X-ray photoelectron spectrum of the Nb 3*d* line from a niobium nitride film with a gallium nitride buffer layer.

Table 3. Layer-by-layer chemical phase profile of the oxidized film NbN/GaN/Sp

N	d, nm	Chemical formula
3	1.23 ± 0.19	$0.48NbO_2 + 0.52Nb_2O_5$
2	5.3 ± 0.4	$0.22NbN + 0.78NbN_x$
1	Thickness not determined	$0.24GaN + 0.76GaN_x$

This corresponds to the measurements by the HRTEM method (pic. 8).

Conclusion

This paper proposes a comprehensive *in situ* method for nondestructive layer-by-layer chemical phase analysis of multilayer inhomogeneous ultra-thin films with sub-nanometer accuracy to the depths of several tens of nanometers. The method is based on the most accurate solution of XPS tasks: subtraction of the background formed by photoelectrons, repeatedly inelastic scattering in a multilayer inhomogeneous medium, and decomposition of the X-ray photoelectron spectral line into phase spectral profiles.

Ultra-thin films of niobium and niobium nitride oxidized in air were analyzed. The layer-by-layer chemical phase profiles of these films are determined. It was found that the layer thickness of a niobium nitride film calculated by the XPS method corresponds to the thickness of the niobium nitride layer determined by the high-resolution TEM method.

Funding

The work was supported by the Ministry of Science and Higher Education of the Russian Federation within the scope of the State Assignment № FSWF-2023-0016.

Conflict of interest

The authors declare that they have no conflict of interest.

References

[1] R.E. Galindo, R. Gago, D. Duday, C. Palacio. Analyt. Bioanalyt. Chem., **396** (8), 2725 (2010). DOI: 10.1007/s00216-009-3339-y
[2] A.V. Lubenchenko, A.A. Batrakov, A.B. Pavolotsky, O.I. Lubenchenko, D.A. Ivanov. Appl. Surf. Sci., **427**, 711 (2018). DOI: 10.1016/j.apsusc.2017.07.256
[3] S. Tougaard. Surf. Sci., **216** (3), 343 (1989). DOI: 10.1016/0039-6028(89)90380-4
[4] S. Tougaard. J. Electron Spectr. Related Phenomena, 178–179, 128 (2010). DOI: 10.1016/j.elspec.2009.08.005
[5] M. Vos, P.L. Grande. Nucl. Instrum. Methods Phys. Res. Section B: Beam Interac-tions with Materials and Atoms, **407**, 97 (2017). DOI: 10.1016/j.nimb.2017.05.064
[6] S. Doniach, M. Sunjic. J. Phys. C: Solid State Phys., **3** (2), 285 (1970). DOI: 10.1088/0022-3719/3/2/010
[7] J.F. Moulder, W.F. Stickle, P.E. Sobol, K.D. Bomben. *Handbook of X Ray Photoelectron Spectroscopy: A Reference Book of Standard Spectra for Identification and Interpretation of XPS Data* (Physical Electronics, 1979)
[8] A.V. Naumkin, A. Kraut-Vass, C.J. Powell. NIST *X-ray Photoelectron Spectroscopy Database* (2008)
[9] A.R. Miedema, R. Boom, F.R. De Boer. J. Less Common Metals, **41** (2), 283 (1975). DOI: 10.1016/0022-5088(75)90034-X
[10] S. Badrinarayanan, S. Sinha. J. Appl. Phys., **69** (3), 1141 (1991). DOI: 10.1063/1.347294
[11] K. Artyushkova, B. Kiefer, B. Halevi, A. Knop-Gericke, R. Schlogl, P. Atanassov. Chem. Commun., **49** (25), 2539 (2013). DOI: 10.1039/C3CC40324F
[12] J. Zemek, J. Houdkova, P. Jiricek, T. Izak, M. Kalbac. Appl. Surf. Sci., **491**, 16 (2019). DOI: 10.1016/j.apsusc.2019.06.083

[13] A. Jablonski. Surf. Sci., **688**, 14 (2019). DOI: 10.1016/j.susc.2019.05.004
[14] S. Krause, V. Afanas'ev, V. Desmaris, D. Meledin, A. Pavolotsky, V. Belitsky, A. Lubenschenko, A. Batrakov, M. Rudziński, E. Pippel. IEEE Transactions Appl. Superconduct., **26** (3), 1 (2016). DOI: 10.1109/TASC.2016.2529432

Translated by A.Akhtyamov